Evaluating the Biological Pump Efficiency of the Last Glacial Maximum Ocean using δ^{13}C

Anne L. Morée[1], Jörg Schwinger[2], Ulysses S. Ninneman[3], Aurich Jeltsch-Thömmes[4], Ingo Bethke[1], Christoph Heinze[1]

[1]Geophysical Institute, University of Bergen and Bjerknes Centre for Climate Research, Bergen, 5007, Norway
[2]NORCE Norwegian Research Centre and Bjerknes Centre for Climate Research, Bergen, 5838, Norway
[3]Department of Earth Science, University of Bergen and Bjerknes Centre for Climate Research, Bergen, 5007, Norway
[4]Climate and Environmental Physics, Physics Institute and Oeschger Centre for Climate Change Research, University of Bern, Bern, Switzerland

Correspondence to: Anne L. Morée (anne.moree@uib.no)

Abstract. Although both physical and biological marine changes are required to explain the 100 ppm lower atmospheric pCO$_2$ of the Last Glacial Maximum (LGM, ~21 ka) as compared to pre-industrial (PI) times, their exact contributions are debated. Proxies of past marine carbon cycling (such as δ^{13}C) document these changes, and thus provide constraints for quantifying the drivers of long-term carbon cycle variability. This modelling study explores the relative roles of physical and biological changes in the ocean needed to simulate an LGM ocean in satisfactory agreement with proxy data, and here especially δ^{13}C. We prepared a PI and LGM ocean model state (NorESM-OC) with full biogeochemistry (including the carbon isotopes δ^{13}C and radiocarbon) and dynamic sea ice. The modelled LGM-PI differences are evaluated against a wide range of physical and biogeochemical proxy data, and show agreement for key aspects of the physical ocean state within the data uncertainties. However, the lack of a simulated increase of regenerated nutrients for the LGM indicates that additional biogeochemical changes are required to simulate an LGM ocean in agreement with proxy data. In order to examine these changes, we explore the theoretical effects of different global mean biological pump efficiencies on the simulated marine biogeochemical tracer distributions. We estimate that (besides changes in ocean circulation) an approximate doubling of the global mean biological pump efficiency from 38 % (PI) to 75 % (LGM) reduces model-proxy biases the most. The remaining absolute model-proxy error in δ^{13}C (which is 0.07 ‰ larger than the 0.19 ‰ data uncertainty) indicates that additional changes in ocean dynamics are needed to simulate an LGM ocean in agreement with proxy data, such as increased aging or volume of Southern Source Waters. Besides that, our theoretical approach of increasing the biological pump efficiency may be too simplified to capture the vertical redistribution of regenerated nutrients – also suggested by a too weak chemocline. Our results underline that only those coupled climate models that contain the processes and/or components that realistically change both ocean circulation and biogeochemistry will be able to simulate an LGM ocean in satisfactory agreement with proxy data – and hence be reliable for use in climate projections. Therefore, future research should aim to identify the exact physical and biogeochemical processes that could have doubled the global mean biological pump efficiency (i.e., the interior regenerated signature) between the PI and LGM, with a likely central role for Southern Source Waters.

1 Introduction

Model and proxy reconstructions of the Last Glacial Maximum (LGM) suggest major redistributions of marine biogeochemical tracers and water masses as compared to pre-industrial (PI) times, as well as lower carbon storage

in both the land biosphere and atmosphere. The culmination of these changes into a ~100 ppm lower LGM atmospheric pCO$_2$ concentration (EPICA Project Members, 2004) has driven extensive research to identify, understand, and quantify the processes contributing to these major atmospheric pCO$_2$ variations (e.g., Broecker, 1982; Broecker and Peng, 1986; Heinze and Hasselmann, 1993; Heinze et al., 2016; Sigman et al., 2010; Adkins,

5   2013; Jeltsch-Thömmes et al., 2019). The oceans are of particular interest as they form the largest carbon reservoir available for atmospheric exchange on millennial timescales, and in addition need to have stored the extra carbon coming from the land biosphere and atmosphere during the LGM. Both physical (circulation, solubility) and biological processes (biological pump efficiency) likely played a role in the differences between the LGM and PI oceans, although their relative importance is under debate: Between ~25 and ~60 % is attributed to biological

10   processes and the remainder to physical changes (Bouttes et al., 2011; Buchanan et al., 2016; Khatiwala et al., 2019).

Here, we explore the relative roles of marine physical and biological changes needed to simulate an LGM ocean in optimal agreement with proxy data. We use the concept of the biological pump efficiency (defined as the ability of marine organisms to consume surface ocean phosphate, or more specifically the ratio of global mean regenerated

15   to total phosphate, Sect. 2.4) to examine its effect on LGM marine biogeochemical tracer distributions in concert with physical changes. The global mean efficiency of the biological pump is strongly and nearly linearly correlated with atmospheric CO$_2$ concentrations (Ito and Follows, 2005) and is considered a key concept to understand the atmospheric CO$_2$ drawdown potential of the ocean (Ödalen et al., 2018) through its influence on the vertical gradient of marine dissolved inorganic carbon (DIC). In our evaluation and discussion, we pay particular attention

20   to the role of Southern Source Waters (SSW, waters originating in the Southern Ocean), which are thought to be a key component in altering ocean interior tracer distributions and glacial atmospheric pCO$_2$ drawdown (e.g., Lynch-Stieglitz et al., 2016; Schmitt et al., 2012; Moy et al., 2019; Sigman et al., 2010; Ferrari et al., 2014; Morée et al., 2018; Khatiwala et al., 2019).

Our work represents the first LGM simulation using a forced isopycnic ocean model (NorESM-OC; Schwinger et

25   al., 2016; Tjiputra et al., 2020), where all atmospheric forcing fields have been adjusted to represent the LGM (Sect. 2). Besides a general ocean circulation model (MICOM), NorESM-OC simulates full biogeochemistry including the ^{13}C and ^{14}C carbon isotopes (model HAMOCC), as well as dynamic sea ice (model CICE) and a prognostic box atmosphere. The simulation of the carbon isotopes is particularly useful here as they i) can be directly compared to data from sediment cores (e.g., Gebbie et al., 2015; Skinner et al., 2017), ii) are influenced

30   by both biological and physical processes (e.g., Broecker and McGee, 2013), iii) give an indication which oceanic regions could be most relevant (Schmitt et al., 2012; Morée et al., 2018; Skinner et al., 2017)), and, given the above, iv) are useful in model evaluation (Schmittner et al., 2013; Braconnot et al., 2012). We focus on the standardized ^{13}C/^{12}C carbon isotope ratio (δ^{13}C; Zeebe and Wolf-Gladrow (2001)), for which relatively many LGM data are available (e.g., Peterson et al., 2014; Oliver et al., 2010). In addition, the ^{14}C/^{12}C carbon isotope ratio

35   (expressed as Δ^{14}C) provides the model with an age tracer (radiocarbon age), which can be used to understand water mass ventilation and circulation rates, and for comparison with reconstructed Δ^{14}C (Skinner et al., 2017; Gebbie and Huybers, 2012). We furthermore evaluate the LGM simulation against proxy and/or model reconstructions of water mass distributions, sea surface temperature, salinity, sea ice extent, export production, vertical nutrient redistribution, atmospheric pCO$_2$, the change in marine dissolved inorganic carbon, and O$_2$ (Sect.

40   3.2). We apply the concept of True Oxygen Utilization (TOU; Ito et al., 2004) instead of Apparent Oxygen

Utilization (AOU) and make use of the explicit simulation of preformed biogeochemical tracers in our model (Tjiputra et al., 2020). This approach makes it possible to separate physical and biogeochemical drivers of the tracer distributions more thoroughly, and accounts for the role of the air-sea carbon disequilibrium pump (Khatiwala et al., 2019). We acknowledge that without a land source of C in our simulated LGM ocean (of ~ 850

5   Gt C, Jeltsch-Thömmes et al., 2019), nor sediments that could alter $CaCO_3$ cycling and long-term organic matter burial (Sigman et al., 2010), we do not expect to simulate the full range of processes contributing to glacial-interglacial pCO_2^{atm} changes. Rather, we include estimates of these carbon reservoir changes in our evaluation of the LGM biological pump efficiency (Sect. 3.3).

The evaluation against proxy data allows us to evaluate both the physical and biological changes needed for

10   simulating the LGM ocean. Notably, in fully coupled paleo Earth System Modelling such as in the most recent Paleo Modelling Intercomparison Project 3 (PMIP3), only two out of nine Earth System Models included marine biogeochemistry in their LGM simulation (IPSL-CM5A-LR (Dufresne et al., 2013) and MIROC-ESM (Sueyoshi et al.,2013)). Earth System Models of intermediate complexity (and coarse resolution ocean model studies) have shown that changes in model (biogeochemical) parameterizations are needed to simulate glacial-interglacial cycles

15   in agreement with proxy records (e.g., Jeltsch-Thömmes et al., 2019; Ganopolski and Brovkin, 2017; Buchanan et al., 2016; Heinze et al., 1991; Heinze and Hasselmann, 1993; Heinze et al., 2016). In our forced ocean model setup, we are able to reveal aspects important for modelling the LGM and relevant for improving the agreement between fully coupled paleo modelling and proxy data. Moreover, our work will help to gain insight in the changes (i.e. physical and biological) needed to simulate a different climate state (such as the LGM) - which also applies

20   to Earth System Model-based climate projections.

2 Methods

2.1 Model description

We apply the ocean carbon-cycle stand-alone configuration of the Norwegian Earth System Model (NorESM) as described by Schwinger et al. (2016), but with several modifications for the next generation NorESM version 2

25   already included. The physical ocean component MICOM (Miami Isopycnic Coordinate Ocean Model; Bentsen et al., 2013) has been updated as described in Guo et al. (2019). The biogeochemistry component HAMOCC (HAMburg Ocean Carbon Cycle model; Maier-Reimer, 1993; Maier-Reimer et al., 2005) adopted for use with the isopycnic MICOM (Assmann et al., 2010; Tjiputra et al., 2013; Schwinger et al., 2016) has undergone a few minor technical improvements (e.g. updated initialisation based on latest data products, additional diagnostic tracers) and

30   employs a new tuning of the ecosystem parameterization as described in Tjiputra et al. (2020).
In addition to these changes, the carbon isotopes (^{13}C and ^{14}C) are implemented in HAMOCC (Tjiputra et al. (2020)), a prognostic box atmosphere is made available for atmospheric CO_2 (including $^{13}CO_2$ and $^{14}CO_2$; Tjiputra et al., 2020), and an LGM setup is made (Sect. 2.2). This is an ocean-only modelling study, where the atmospheric forcing is prescribed from a data set (except atmospheric CO_2, $\delta^{13}C$ and $\Delta^{14}C$, which evolve freely; Sect. 2.2). All

35   simulations in this study are done without the sediment module of HAMOCC (this is done in order to avoid prohibitively long spin-up times, especially for the carbon isotopes; an acceleration method for the model spin-up including interactive water column-sediment interaction is work in progress for a separate manuscript). Applying the current set-up, detritus arriving at the sediment-water interface is evenly redistributed over the entire water

column, while opal and $CaCO_3$ are dissolved immediately in the bottom-most mass containing layer. Riverine input of carbon and nutrient is also turned off. Furthermore, nitrogen deposition, denitrification and nitrogen fixation are excluded from our simulations, as these processes cause a long-term drift in the alkalinity inventory of the ocean (and thereby the pCO$_2$ of the prognostic atmosphere).

5 The two main isotopes of carbon, ^{13}C and ^{14}C, are newly implemented in HAMOCC (Tjiputra et al., 2020). The model includes fractionation during air-sea gas exchange and photosynthesis, as well as radiocarbon decay. Fractionation during $CaCO_3$ formation is small as compared to the effects of air-sea gas exchange and photosynthesis, as well as uncertain (Zeebe and Wolf-Gladrow, 2001) and is therefore omitted (e.g., Schmittner et al., 2013; Lynch-Stieglitz et al., 1995). Air-sea gas exchange fractionation (~8-11 ‰) is a function of surface ocean

10 temperature and the CO_3^{2-} fraction of total DIC such that fractionation increases with decreasing temperatures (Zhang et al., 1995; Mook, 1986). Biological fractionation (~19 ‰) increases surface water $\delta^{13}C$ of DIC while producing low-$\delta^{13}C$ organic matter. In the interior ocean, this light isotope signal from organic matter is released back into the water column during remineralization and respiration, thereby creating a vertical gradient. HAMOCC applies the parameterization by Laws et al. (1997), where the biological fractionation ε_{bio} depends on the ratio

15 between phytoplankton growth rate and the aqueous CO_2 concentration. For ^{14}C, each fractionation factor is set to the quadratic of the respective ^{13}C value (i.e., $\alpha_{14C} = \alpha^2_{13C}$). In addition, ^{14}C is radioactive and decays with a half-life of 5730 years to [14]N.

In order to evaluate the carbon isotopes against observations, we derive $\delta^{13}C$ and $\Delta^{14}C$. $\delta^{13}C$ is calculated using the standard equation $\delta^{13}C = \left(\frac{^{13}C/^{12}C}{(^{13}C/^{12}C)_{standard}} - 1\right) * 1000$ ‰, where $(^{13}C/^{12}C)_{standard}$ is the Pee Dee

20 Belemnite standard ratio (0.0112372; Craig (1957)). $\Delta^{14}C$ is calculated by standardizing DI[14]C following $\delta^{14}C = \left(\frac{^{14}C/C}{(^{14}C/C)_{standard}} - 1\right) * 1000$ ‰, where $(^{14}C/C)_{standard}$ is the NBS standard (1.170·e^{-12}; Orr et al., 2017). $\Delta^{14}C$ is then calculated from $\delta^{14}C$, following $\Delta^{14}C = \delta^{14}C - 2 * (\delta^{13}C + 25) * (1 + \frac{\delta^{14}C}{1000})$. $\Delta^{14}C$ age presented in this study is derived from $\Delta^{14}C$ of DIC following $(\Delta^{14}C_{age} = -8033 * \ln(-8033 * \Delta^{14}C/1000) + 1)$ and is based on calibrated $\Delta^{14}C$ of DIC using an atmospheric value of 0 ‰ for both the LGM and PI spinup (Tjiputra et al.,

25 2020). This approach facilitates comparison with the radiocarbon disequilibrium data by Skinner et al. (2017).

2.2 Last Glacial Maximum set-up

Several adjustments were made to the model in order to obtain a LGM circulation field. First, the land-sea mask and ocean bathymetry were adjusted for the ~120 m lower sea level in the LGM caused by the increased land ice volume as compared to the PI. Following the PMIP4 guidelines in Kageyama et al. (2017) the Bering Strait is

30 closed, and the Canadian Archipelago (including Borrow Strait and Nares Strait), Barents Sea, Hudson Bay, Black Sea, Red Sea, as well as the Baltic and North Seas are defined as land in the LGM. The PI land-sea mask formed the basis for the LGM land-sea mask, through shifting the PI bathymetry 116 m upwards. If the resulting depth in a grid cell was between 0-25 meters, the depth was set to 25 m and negative depths were set to land grid points. After this, any channels with a width of only one grid cell were closed off as well, as these inhibit sea ice movement

35 in the sea ice model causing unrealistic sea ice build-up. LGM freshwater runoff is routed to the nearest ocean grid cell but otherwise unadjusted.

Changes in isopycnal densities and sea surface salinity restoring are applied in the LGM model setup in order to ensure an adequate vertical model resolution and ocean circulation. A net LGM increase in density due to

decreased ocean temperatures and increased ocean salinity required increasing all 53 isopycnal layer densities by 1.3 kg m^{-3} in the LGM setup as compared to the PI model setup. NorESM-OC uses salinity restoring to avoid long-term drift away from a predefined SSS state. Here, this predefined state is chosen, consistent with the atmospheric forcing (see below) as the mean of the LGM minus PI SSS anomaly modelled by PMIP3 models added to a PI

5   SSS climatology. However, the unadjusted application of the PMIP3-based SSS anomaly caused an Atlantic water mass distribution and overturning strength in poor agreement with proxy reconstructions (SM 2). Earlier studies have shown a high sensitivity of models to SSS restoring, especially in the North Atlantic (Rahmstorf, 1996; Spence et al., 2008; Bopp et al., 2017). Indeed, the density contrast between Northern and Southern source waters drives the simulated Atlantic Meridional Overturning Circulation (AMOC) strength in many of the PMIP2 models

10   (Weber et al., 2007), and is therefore important for the simulation of overturning strength in agreement with proxy records. Therefore, we adjust the SSS restoring present in NorESM-OC to obtain a circulation field in better agreement with proxy reconstructions: In addition to the PMIP3-based SSS anomaly, we apply a region of -0.5 psu in the North Atlantic and +0.5 psu in the Southern Ocean (for specifics, see SM 1), as done similarly by Winguth et al. (1999) or through freshwater fluxes by Menviel et al. (2017) and Bopp et al. (2017).

15   An atmospheric LGM forcing for NorESM-OC was created by adding anomalies (relative to the pre-industrial state) derived from PMIP3 models (Morée and Schwinger, 2019; version 1) to the CORE Normal Year Forcing (NYF; Large and Yeager, 2004). The use of mean PMIP/CMIP anomalies to force stand-alone models is a standard approach that has been tested before (Mitchell et al., 2017; Chowdhury and Behera, 2019; Muglia et al., 2015; Muglia et al., 2018). Through this approach, the effect of the presence of sea ice on the atmospheric state is included

20   in the forcing, but the sea ice model handles the actual formation/melt of sea ice. Compared to the PI CORE-NYF, the LGM forcing over the ocean has a lower specific humidity (especially in the tropics), decreased downwelling longwave radiation, precipitation and air temperature, and a heterogeneous change in downwelling shortwave radiation and zonal and meridional winds. In addition to the adjustments to the NYF, the dust fluxes of Lambert et al. (2015) are used in the LGM model setup, following PMIP4 guidelines (Kageyama et al., 2017). The PI setup

25   uses the Mahowald et al. (2006) dust dataset.

2.3 Initialization and tuning

All marine biogeochemical tracers were initialized in the LGM as done for the PI spin-up using the WOA and GLODAPv2 data sets. For the LGM, consistent with the decreased ocean volume, all biogeochemical tracer concentration are increased at initialization by 3.26 %. Similarly, ocean salinity is uniformly increased by 1 psu,

30   following PMIP recommendations. The carbon isotopes (Sect. 2.1) are only enabled after an initial spin-up of the model in order to first obtain reasonably stabilized total carbon tracer distributions. DI^{13}C is initialized after 1000 years using the correlation between δ^{13}C and apparent oxygen utilization (AOU) in combination with the model's DIC distribution. We applied the δ^{13}C:AOU relationship of the pre-industrial Eide et al. (2017) data ($\delta^{13}C_{PI} = -0.0075 \cdot AOU + 1.72$) and converted to absolute model ^{13}C using model DIC and AOU. As this approach uses

35   the model's 'native' AOU and DIC, the equilibration time of δ^{13}C was reduced as compared to initialisation with a δ^{13}C data product such as that of Eide et al. (2017). Model DI^{14}C is initialized after 4000 years by first calculating δ^{14}C using a combination of pre-industrial δ^{13}C (Eide et al., 2017) (with the missing upper 200m copied from 200m depth to all empty surface layers) and the observational-based estimate of pre-industrial Δ^{14}C (Key et al., 2004). Then, model DI^{14}C is derived from the δ^{14}C by rewriting and solving the standardization equation ($\delta^{14}C =$

$\left(\frac{^{14}C/C}{(^{14}C/C)_{standard}} - 1\right) * 1000$ ‰, with model DIC as C). Subsequently, isotopic DOC, POC, phytoplankton C, and zooplankton C are initialized as done for the corresponding total carbon variable, but multiplied with 0.98 (as an estimate of the photosynthetic fractionation effect) and the respective $DI^{13}C/DI^{12}C$ or $DI^{14}C/DI^{12}C$ ratio. Isotopic $CaCO_3$ is initialized as for total carbon, multiplied with $DI^{13}C/DI^{12}C$ or $DI^{14}C/DI^{12}C$, as we do not consider

5   fractionation during $CaCO_3$ formation.

The prognostic atmospheric pCO_2 is initialized at 278 ppm for both spin-ups. At initialization of the carbon isotopes, atmospheric $\delta^{13}C$ is set to -6.5 ‰ and atmospheric $\Delta^{14}C$ is set to 0 ‰. Atmospheric pCO_2 at the time of initialization is then used to calculate the absolute ^{13}C and ^{14}C model concentrations ($^{13}C^{atm}$ and $^{14}C^{atm}$, in ppm).

Two main spin-ups have been made with NorESM-OC: One for the LGM and one for the PI, designed as described

10   in Sect. 2.1-2.3. Both the PI and LGM simulations are run for a total of 5600 years.

2.4 Analysis of the biological pump efficiency

Here, we explore the effect of an increase in the global mean biological pump efficiency ($\overline{BP_{eff}}$, Eq. 1), which we define, following Ito and Follows (2005), as the ratio between global mean regenerated phosphate ($\overline{PO_4^{reg}}$) and global mean total phosphate ($\overline{PO_4}$).

15    $$\overline{BP_{eff}} = \overline{PO_4^{reg}}/\overline{PO_4} \qquad (1)$$

Regenerated phosphate is calculated as the difference between total phosphate and preformed phosphate (PO_4^{pref}). PO_4^{pref} is explicitly simulated in the model (Tjiputra et al., 2020), and represents phosphate that leaves the mixed layer in inorganic form (unutilized by biology).

We work with the global mean value of $\overline{BP_{eff}}$ as this governs pCO_2^{atm} (Ito and Follows, 2005; Ödalen et al., 2018).

20   However, we note that major local differences in the ratio of regenerated to total phosphate exist in the ocean, for example between North Atlantic Deep Water (high-ratio) and Antarctic Bottom Water (low-ratio) (Ito and Follows, 2005; DeVries et al., 2012), which thus indicate the differences in potential to sequester carbon and nutrients in the ocean interior. Here, changes in $\overline{BP_{eff}}$ are calculated in a theoretical framework (off-line) to better understand the LGM redistribution of carbon between the land, atmosphere and ocean, and its effects on marine

25   biogeochemistry (and corresponding proxy data). Our approach also allows us to give an upper estimate of the $\overline{BP_{eff}}$ of the LGM ocean.

Simulated $\overline{BP_{eff}}$ can be adjusted to any assumed $\overline{BP_{eff}}$ by changing $\overline{PO_4^{reg}}$ ($\overline{PO_4^{reg}}_{new} = \overline{BP_{eff}}_{new} \times \overline{PO_4}$). The assumed change in PO_4^{reg} (ΔPO_4^{reg}) is used to estimate the effects on DIC, O_2 and $\delta^{13}C$ using the following relationships:

30    $$O_2^{new} = O_2 - \Delta PO_4^{reg} \times r_{O:P} \qquad (2)$$

$$DIC^{new} = DIC + \Delta PO_4^{reg} \times r_{C:P} \qquad (3)$$

$$\delta^{13}C^{new} = \delta^{13}C - R_{\delta^{13}C:PO_4^{reg}} \times \Delta PO_4^{reg} \qquad (4)$$

Model Redfield ratios $r_{O_2:P}$ and $r_{C:P}$ are set to 172 and 122, respectively (following Takahashi et al., 1985). $R_{\delta^{13}C:PO_4^{reg}}$ is the slope of the $\delta^{13}C:PO_4^{reg}$ relationship, which is found to be 0.67 in the model (R^2=0.76).

35   The spatial distribution of ΔPO_4^{reg} is an important consideration. We therefore explore ΔPO_4^{reg} by applying three different methods: The first method (method 'add') equally distributes the mean change in ΔPO_4^{reg} over the entire

ocean ($PO_4^{reg}{}_{new} = PO_4^{reg}{}_{model} + \overline{\Delta PO_4^{reg}}$). The second method (method 'factor') takes into account the original distribution of $PO_4^{reg}{}_{model}$ (by calculating $\overline{\Delta PO_4^{reg}} = \overline{PO_4^{reg}}{}_{new} / \overline{PO_4^{reg}}{}_{model}$ and calculating for every grid cell $PO_4^{reg}{}_{new} = PO_4^{reg}{}_{model} \times \overline{\Delta PO_4^{reg}}$). The third method is as the first, additive, method but only adding the extra regenerated tracers to SSW as determined from the conservative PO tracer (method 'SSW', see Sect. 3.2 for the

5   LGM PO tracer distribution).

It is important to note that $\overline{BP_{eff}}$ can be changed by several processes: through the soft- and hard tissue biological pumps, the solubility pump (Heinze et al., 1991; Volk and Hoffert, 1985) and by changes in the physical carbon pump (circulation/stratification of the water column).

3 Results and discussion

10   The results presented in Sect. 3.1 and Sect. 3.2 are the annual mean climatologies over the last 30 years of the 5600-year PI and LGM spin-ups. We present an evaluation of the PI (Sect. 3.1) and LGM (Sect. 3.2) spin-ups and compare the latter to proxy reconstructions, and discuss the LGM-PI changes in a theoretical framework exploring the efficiency of the biological pump (Sect. 3.3).

3.1 The simulated pre-industrial ocean

15   The simulated pre-industrial ocean state has a maximum AMOC strength of ~18 ± 0.5 Sv north of 20° N, which compares favourably to the mean observational estimates of 17.2-18.7 Sv (Srokosz and Bryden, 2015; McCarthy et al., 2015), especially when noting the wide range of modelled AMOC strengths in similar forced ocean setups (Danabasoglu et al., 2014). The interannual variability of the simulated AMOC is small compared to observations (about ±4 Sv; Srokosz and Bryden, 2015), due to the annually repeating forcing. Drake Passage transport is

20   simulated at ~114 Sv, lower than recent observational estimate of 173.3 ± 10.7 Sv (Donohue et al., 2016). The depth of the transition between the upper and lower overturning cells at 30° S lies at ~2700 m, comparable to other model estimates (Weber et al., 2007). Temperature biases are generally modest (smaller than ± 1.5°C) for most of the ocean above 3000m, except for a warm bias related to a too deep tropical and subtropical thermocline. At depth (>3000 m) there is a widespread cold bias that originates from the Southern Ocean (too much deep mixing and

25   associated heat loss to the atmosphere). Salinity biases are generally small, except for a positive bias related to a too strong Mediterranean outflow at mid-depth in the Atlantic. Furthermore, the ocean is ~0.2-0.3 psu too fresh at depths over ~3 km. The mixed layer depth (MLD) is generally simulated too deep (compared to the observational estimates of De Boyer Montégut et al. (2004)). In the high latitudes, winter month MLD biases in excess of 200 metres are present in our model. In low latitudes, MLD is about 20 metres too deep year-round. The simulated

30   biogeochemistry of the PI ocean is described in more detail in Schwinger et al. (2016) although there have been some improvements due to the model updates mentioned above as described in Tjiputra et al. (2020). Some features of relevance for this study are summarized here: The spatial pattern of primary production (PP) compares well with observation-based estimates with the exception of the tropical Pacific upwelling, where PP is too high, and the subtropical gyres where PP is generally too low. Because of too high PP and export in the equatorial Pacific,

35   a far too large oxygen minimum zone (OMZ) with elevated concentrations of regenerated phosphate develops in the model. Otherwise, the global nutrient concentrations are in reasonable agreement with modern observations

(WOA, Glodapv2). $\overline{BP_{eff}}$ is 38 % for the simulated PI ocean, in good agreement with observational estimates of 32-46 % (Ito and Follows, 2005; Primeau et al., 2013).

3.2 The simulated LGM ocean

3.2.1 The physical ocean state

5   Proxy-based reconstructions describe an LGM circulation that includes a shoaling of the upper circulation cell in the Atlantic (Glacial NADW) and expansion and slow-down of a cooler and more saline lower circulation cell (Glacial AABW; Adkins, 2013; Sigman et al., 2010; Ferrari et al., 2014). In this study, we assume these aspects of the LGM ocean to be qualitatively correct, and therefore aim for a model simulation in agreement with these features. We note that discussion continues as to the magnitude and veracity of these change (e.g., Gebbie, 2014).

10   Most reconstructions estimate a weakened AMOC for the LGM as compared to the PI state, although estimates vary between a 50 % weakening and an invigoration of AMOC (McManus et al., 2004; Kurahashi-Nakamura et al., 2017; Böhm et al., 2014; Lynch-Stieglitz et al., 2007; Muglia et al., 2018). The maximum overturning strength north of 20° N simulated by NorESM-OC is 15.6 Sv (~7 % weaker than simulated for our PI ocean, which we attribute to our adjustments and tuning of the salinity restoring). Higher uncertainties are involved with

15   reconstructions of the strength of the Antarctic Circumpolar Current (ACC), with consensus leaning towards a slight invigoration (Lynch-Stieglitz et al., 2016; Lamy et al., 2015; McCave et al., 2013; Mazaud et al., 2010; Buchanan et al., 2016). We simulate a Drake Passage transport of 129 Sv, which is about 13 % stronger than simulated for the PI ocean. The simulated transition between the Atlantic overturning cells shoals by ~350m, which falls within the uncertainty of reconstructions (Gebbie, 2014; Adkins, 2013; Oppo et al., 2018) (Fig. S5).

20   Specifically, the transition lies well above the main bathymetric features of the Atlantic Ocean in our LGM simulation (as visible from the transition line in the PO tracer; Fig. 1). This could have been an important feature of the glacial Atlantic water mass configuration due to reduced mixing along topography (Adkins, 2013; Ferrari et al., 2014) - i.e., shifting water mass boundaries away from the regions of intense internal mixing increases chemical and tracer stratification. The changes in water mass circulation cause an increased SSW volume

25   contribution to the Atlantic and Pacific basins, as visible from the conservative PO tracer (Fig. 1, and Fig. S4 for Pacific) (Broecker, 1974), and in agreement with proxy reconstructions. Radiocarbon age increases at depth (Fig. 1c and Fig. S4), with a global volume-weighted mean increase of 269 years. This is low compared to the estimate of Skinner et al. (2017) of 689±53 years, and we find the majority of our radiocarbon age bias to lie at depth in the Atlantic (not shown) indicating too strong ventilation and/or biased equilibration of these waters (which have a

30   southern source, Fig 1a-b). Furthermore, SSW salinity increases (Fig. S6) – also in good agreement with proxy reconstructions (Adkins, 2013). Also relevant for the water mass circulation as well as marine biogeochemistry, are the low LGM atmospheric temperatures that cause a mean ocean temperature decrease of 1.9 °C in the model. This is less than the 2.57 ± 0.24 °C estimated from proxy reconstructions of mean ocean temperature (Bereiter et al., 2018), likely because the SSW may not carry a strong enough temperature decrease from the atmosphere into

35   the interior ocean in our simulation (Fig. S7) – implying an underestimation of negative buoyancy fluxes. While the differences between our simulated LGM-PI changes in SST (Fig. S8) do not exhibit the same amount of heterogeneity as observed in proxy reconstructions (MARGO Project Members, 2009), the simulated mean SST change (-1.97 °C) seems reasonable when taking into account the uncertainty of SST reconstructions (MARGO Project Members (2009) estimate -1.9 ± 1.8 °C; Ho and Laepple, 2015). Further, the general pattern of stronger

SST cooling outside of the polar regions is captured which is important for the air-sea disequilibrium pump (Khatiwala et al., 2019). We simulate an increase in Southern Ocean sea ice cover for both summer and winter (Fig. S9), but less than is inferred from proxy-based reconstructions for the LGM (Gersonde et al., 2005) – similar to PMIP models (Roche et al., 2012). Southern Ocean sea ice may have played a major role in LGM marine

5   biogeochemistry and interior ocean carbon storage (Ferrari et al., 2014; Marzocchi and Jansen, 2017; Stephens and Keeling, 2000), and could therefore explain some of the model biases. Examples are the lack of stratification in the Southern Ocean which is thought to be driven by brine rejection from sea ice (Jansen, 2017), and affect air-sea equilibration of biogeochemical tracers such as DIC and O_2 (Gottschalk et al., 2016a).

10   **3.2.2. The biogeochemical ocean state**

Proxies for the past biogeochemical state of the ocean (such as export production, oxygen concentrations, $\delta^{13}C$) allow us to make a further evaluation of our simulated LGM ocean (Fig. 2). The global mean efficiency of the biological pump $\overline{BP_{eff}}$ decreases from 38 % in the PI simulation to 33 % in the LGM simulation, as opposed to reconstructions which infer an increased regenerated signature in the interior ocean (Jaccard et al., 2009; Umling

15   et al., 2018; Freeman et al., 2016). The simulated increase in preformed phosphate (Fig. 2) represents an increased (but unused) potential for the ocean to draw down atmospheric pCO_2 (Ödalen et al., 2018). We can attribute our simulated decrease in $\overline{BP_{eff}}$ to the increase in SSW volume (Fig. 1), as SSW has a low regenerated signature (Ito and Follows, 2005). Despite the decrease in $\overline{BP_{eff}}$, simulated pCO_2^{atm} is 21 ppm lower in our LGM setup as compared to the PI setup. We attribute this change to the net effect of the i) smaller ocean volume, causing the

20   concentration of alkalinity, DIC and salinity and a reportedly ~16 ppm pCO_2^{atm} increase (Sarmiento and Gruber, 2006), and ii) the decrease in water temperature, which drives a pCO_2^{atm} drawdown of ~30 ppm (Sigman and Boyle, 2000). As we made no additional changes to the marine biogeochemical model (except for a LGM dust input field), and have no sediment or land model included in our simulation, the ~20 ppm pCO_2^{atm} drawdown as well as limited changes in regenerated nutrient inventories is expected and found in earlier studies (e.g., Buchanan

25   et al., 2016). Similarly, the atmospheric $\delta^{13}C$ change due to glacial land-vegetation loss is not simulated because we only simulate the ocean.

Simulated changes in Atlantic total phosphate (Fig. 2) agree well qualitatively with reconstructed nutrient redistributions, which describe a deep ocean nutrient increase and mid-to surface decrease (Buchanan et al., 2016; Gebbie, 2014; Marchitto and Broecker, 2006; Oppo et al., 2018). North Pacific waters >2.5 km depth exhibit a

30   lower LGM phosphate (and DIC) as compared to the PI, due to the lack of accumulated regenerated phosphate (Fig. S10). In agreement with the expectation of increased interior carbon storage, simulated interior DIC increases - especially in SSW (Fig. 2). As for phosphate, this increase is driven by the physical carbon pump only, through higher saturation of surface DIC in the Southern Ocean driven by lower T and increased alkalinity (not shown). However, the biases in simulated O_2 and $\delta^{13}C$ LGM-PI changes and their respective proxy reconstructions are

35   large (Fig. 2). Any mismatch in the absolute values of $\delta^{13}C$ is not shown here because we compare LGM-PI differences in both the sediment cores and model. In line with decreased remineralisation and increased O_2 solubility due to lower temperatures in the model, O_2 concentrations increase throughout the ocean (Fig. 2). There is a notable difference between Northern and Southern end-members in the Atlantic: Northern-source deep waters have increased O_2 concentrations due to physical O_2 pumping (colder waters have higher O_2 solubility) as visible

40   in preformed O_2, while SSW O_2 increases due to a lack of remineralisation at depth due to low oxygen utilization

(Fig. 3). The general increase in O_2 concentrations, mostly due to the lack of biological O_2 consumption at depth (Fig. 3), is in disagreement with proxy reconstructions (Jaccard and Galbraith, 2011) and shows the missing regenerated nutrients should mostly come from lacking biological processes (remineralization). $\delta^{13}C$ of DIC is governed by both ocean circulation (ventilation rate) and the efficiency of the biological pump (respiration rate), and their relative importance depends on location (Gruber et al., 1999; Schmittner et al., 2013; Eide et al., 2017). As for O_2, the overall increase in simulated $\delta^{13}C$ of DIC contradicts $\delta^{13}C$ records from sediment cores, in which the strengthening of the vertical gradient is a main feature (Fig. 2). Deep $\delta^{13}C$ and its vertical gradient is for an important part governed by biological processes (Morée et al., 2018). As a last comparison, we evaluate our modelled changes in export production against proxy data, even though such data have poor global coverage and large spatial heterogeneity, and are largely qualitative (Kohfeld et al., 2005). LGM export production generally decreases outside of upwelling zones in our model (Fig. 4) and increases in upwelling zones (model and proxy data, Fig. 4). We conclude that the simulated export production increase may be too weak in the sub-Antarctic and is lacking in the tropical Atlantic (Fig. 4). Especially Southern Ocean export production has a large potential to affect interior and lower latitude nutrient and DIC concentrations (Sarmiento et al., 2004; Primeau et al., 2013), and likely contributes to the simulated low $\overline{BP_{eff}}$ and low-regenerated signature in the biogeochemical tracer distributions. Considering the large influence of SSW nutrient supply on lower latitude productivity we anticipate a key role for SSW here - as supported by proxy data (e.g., Winckler et al., 2016; Costa et al., 2016), although local changes in iron fertilization may play an additional role depending on local iron limitation (e.g., Oka et al., 2011).

3.3 The potential of the biological pump

A decrease in pCO$_2^{atm}$ and increase in regenerated nutrients, despite an increase in low regenerated nutrient SSW volume, is likely to occur through the increase of BP_{eff} (and thus regenerated nutrients) of SSW (Jaccard et al., 2009). In addition, an increase in the (Southern Ocean) air-sea disequilibrium of DIC may have kept more carbon sequestered in the deep ocean, through increased stratification and inhibition of air-sea gas exchange by for example sea ice (Jansen, 2017). An increase in the regenerated signature of northern source water would have further contributed to a global increase in regenerated carbon and nutrients in the interior ocean (Yu et al., 2019), although occupying a smaller volume. As natural preformed concentrations in SSW are high (Ito and Follows, 2005), there is a high potential for these waters to obtain a stronger regenerated signature, and thereby facilitate pCO$_2^{atm}$ drawdown (Ödalen et al., 2018). Our model results for the LGM-PI change in O_2 and $\delta^{13}C$ show a strong miss-match with proxy records (Sect. 3.2.2 and Fig. 2). Here, we explore the effect of a theoretical ('offline') increase of regenerated nutrients in the ocean, by increasing regenerated phosphate and updating O_2, DIC and $\delta^{13}C$ accordingly (Sect. 2.4). The increase is projected on the same simulated physical ocean state presumed to represent LGM conditions (i.e. Sect 3.2.1). To the extent that this state represents true glacial conditions, it allows for an assessment of the magnitude and nature of marine biogeochemical changes needed for lowering LGM pCO$_2^{atm}$. In our approach, the additional regenerated phosphate is taken from preformed phosphate, thus leaving the total phosphate inventory unchanged. Proxy reconstructions of global LGM phosphate, however, show that LGM phosphate was redistributed as well as elevated (Tamburini and Föllmi, 2009; Filippelli et al., 2007). As we consider a closed system (no sediments or land input of phosphate or other elements), only redistributions of phosphate can be captured in our model setup.

We compare the mean error between the model and the δ^{13}C proxy data across a wide range of $\overline{BP_{eff}}$ (20-100 %, Fig. 5), and for the different methods of adding regenerated δ^{13}C (Sect. 2.4). Besides the physical and biogeochemical constraints and evaluation (Sect. 3.2), we also estimate the LGM-PI change in marine DIC (ΔDIC) by applying the Bern3D Earth System Model of Intermediate Complexity v.2.0s following Jeltsch-Thömmes et al.

5   (2019) (SM 3). Mean ΔDIC is ~4000 Gt C (1 sigma range: 3350 to 4480 Gt C) based on the constraints given to the Bern3D model (pCO$_2^{atm}$, δ^{13}C^{atm}, marine δ^{13}C of DIC, and deep equatorial Pacific CO$_3^{2-}$). Contributions to ΔDIC as evaluated in the framework of Jeltsch-Thömmes et al. (2019) arise from removal of carbon from the ocean by sedimentation-weathering imbalances, coral reef growth, increase of the terrestrial carbon storage, and increase in atmospheric CO$_2$ from the LGM to PI. The wide spread in the ΔDIC estimate by the Bern3D model

10 highlights uncertainties connected to particularly the weathering-burial cycle of carbon over glacial-interglacial timescales.

Using NorESM-OC, the best fit between the modelled and sediment core LGM-PI changes in δ^{13}C is found for a $\overline{BP_{eff}}$ of 75 % (Fig. 5). A $\overline{BP_{eff}}$ of 75 % would lead to the adjusted tracer distributions shown in Fig. 6 (applying Eq. 2-4). This is true for the approach 'factor' (described in Sect. 2.4), indicating that taking the distribution of the

15 original simulated LGM PO$_4^{reg}$ and strengthening that regenerated signal gives the best agreement with sediment core data. The $\overline{BP_{eff}}$ of 75 % corresponds to a LGM-PI ΔDIC of ~1850 Gt C. This ΔDIC estimate falls below the overall range (2400 to 5500 Gt C) given by the Bern3D model and its constraints. If using only one of the above constraints, however (pCO$_2^{atm}$, δ^{13}C^{atm}, marine δ^{13}C of DIC, and deep equatorial Pacific CO$_3^{2-}$), the ΔDIC estimate of ~1850 Gt C lies in the range of Bern3D results (see SM 3 for details). Furthermore, we expect that values given

20 by the Bern3D model likely lie at the high end of estimates (see also discussion in Jeltsch-Thömmes et al., 2019 and SM3). Using their idealized model setup, Schmittner and Somes (2016) estimated a LGM $\overline{BP_{eff}}$ of 54-59 % (41 % in PI) and a ΔDIC of 590-790 Gt C by exploring the effects of a uniform change in the maximum growth rate of phytoplankton. A direct comparison between these studies is complicated by the large differences between the models, but the differences indicate remaining uncertainties in the magnitude of both ΔDIC and LGM $\overline{BP_{eff}}$.

25 Nevertheless, LGM $\overline{BP_{eff}}$ seems to have been about 18 (i.e. 59-41) % and up to 37 (i.e. 75-38) % higher than in the PI. We note that the total marine ΔDIC (~1850 Gt C) estimate points towards a central role for the Pacific basin to store glacial carbon, if we consider Atlantic LGM storage >3 km depth to be in the order of 50 Gt C (Yu et al., 2016).

In addition to evaluating the model-data fit of δ^{13}C, we evaluate the effect of the tracer adjustments on O$_2$. The

30 decrease in O$_2$ for an adjusted $\overline{BP_{eff}}$ (Fig. 6) shows better agreement with qualitative proxy data in the Atlantic (Compare Figs. 2 and 6; Jaccard and Galbraith, 2011) as well as the estimated 175±20 µmol kg^{-1} LGM-PI decrease in Sub-Antarctic Atlantic bottom-water (Gottschalk et al., 2016a). Absolute LGM O$_2$ (Fig. S11) would decrease to sub-zero O$_2$ concentrations in the North Pacific (ca. -100 µmol kg^{-1}), which is of a similar magnitude as the size of the PI model-observation bias in this area (Tjiputra et al., 2020), but may be too extreme as indicated by

35 qualitative proxy data that describe a LGM-PI O$_2$ increase for the North Pacific above 3 km depth (Fig. S10; Jaccard and Galbraith, 2011). An increase in denitrification could have played a role here, but cannot be evaluated in our model setup. Additional (quantitative) estimates of LGM-PI O$_2$ for major water masses would thus help to provide further constraints on LGM $\overline{BP_{eff}}$.

Our mean absolute error in δ^{13}C decreases from 0.67 ‰ for the original LGM state estimate (Fig. 2) to 0.26 ‰ for

40 the 75% $\overline{BP_{eff}}$ ocean (Fig. 5 and 6). The remaining absolute δ^{13}C error is therefore 0.07 ‰ larger than the proxy

data uncertainty. This remaining model-data $\delta^{13}C$ mismatch of 0.07 ‰ (Fig. 5) as well as the possibly too low Pacific O_2 (Fig. S10) indicate that projecting changes in $\overline{BP_{eff}}$ onto the simulated glacial circulation field still does not fully align with the actual LGM state - despite exploring different approaches for the redistribution of the regenerated nutrients (Sect. 2.4). Specifically, even though a 75 % $\overline{BP_{eff}}$ and the reorganised circulation captures

5 most of the magnitude of the LGM-PI $\delta^{13}C$ change, the strength of the glacial chemocline (the vertical $\delta^{13}C$ gradient) remains too weak (Fig. 6). Other modelling studies of the glacial ocean show similar biases (e.g., Heinze et al., 2016; Schmittner and Somes, 2016). This suggests additional processes, which would allow stronger chemical stratification between intermediate and deep waters, are missing in the model(s) and are not explained in a simple way by intensification of the biological pump or our simulated changes in circulation. We recognize that

10 optimizing the model $\overline{BP_{eff}}$ to additional (quantitative) proxies such as the nitrogen isotopes could provide more constraints (Schmittner and Somes, 2016).

Here, we discuss several processes that could contribute to the remaining model-proxy error. First, our results may indicate that the water mass production processes in the model are not (yet) fully adequate. Interior $\delta^{13}C$ is influenced by the source of deep waters as well as intermediate waters, the extent of deep convection as well as

15 mixing processes between interior water masses (e.g., Duplessy et al., 1988), partly on spatial and temporal scales possibly not resolved by our model. The PI simulation of a generally too deep Southern Ocean MLD as well as Southern Ocean- attributed model-observational biases in biogeochemical tracers (Sect. 3.1; Tjiputra et al., 2020) suggest that deep water formation processes indeed are not simulated in full agreement with observational data. The lack of a reliable glacial freshwater forcing is likely to be partly responsible for errors in the LGM simulation.

20 Too strong exchange (mixing) in the LGM ocean between the deep and intermediate waters in models could also maintain a too weak glacial chemocline. Our simulated SSW radiocarbon ages are too young compared to reconstructions (Fig. 1), consistent with inadequate isolation of these waters in the simulation. Aging of these SSW could increase the regenerated signature in these waters (consuming O_2, and decreasing $\delta^{13}C$ of DIC) and steepen the chemocline while additionally improving agreement with the Bern3D model ΔDIC estimate and radiocarbon

25 age. The simulation of increased Southern Ocean sea ice extent and/or formation rate (Nadeau et al., 2019) may be a key player for improving simulations of a more stratified and isolated SSW (Ferrari et al., 2014; Jansen 2017), which would create older waters with higher regenerated signatures and increase the air-sea disequilibrium of biogeochemical tracers such as DIC and O_2 (Gottschalk et al., 2016a) further lowering atmispheric CO_2 (Khatiwala et al., 2019).

30 **4 Conclusions**

We present a model simulation of the pre-industrial and Last Glacial Maximum (LGM) oceans. We use the simulations to explore the relative roles of physical and biological marine changes needed to simulate an LGM ocean in satisfactory agreement with proxy data. Despite the good agreement between (qualitative and quantitative) proxy reconstructions and our simulation of different LGM and pre-industrial (PI) ocean circulation,

35 our model is unable to simulate the complete set of biogeochemical changes implied by proxy data. Therefore, our results (mainly the lack of increased regenerated nutrients) confirm the idea that both biogeochemical (beyond those represented by the model) and physical changes must have been at play in the ocean to create the LGM pCO$_2^{atm}$ drawdown (Heinze et al., 2016; Bouttes et al., 2011; Buchanan et al., 2016). Comparison between a range

of qualitative and quantitative proxy data and simulated biogeochemical tracers (specifically total dissolved inorganic carbon, regenerated phosphate, True Oxygen Utilization, O_2 and $\delta^{13}C$) reveals that there is a too small signature of regenerated nutrients in our simulated LGM ocean. We conduct a theoretical exploration of the effects of changes in the global mean biological pump efficiency and quantify its effect on the global mean absolute error between simulated $\delta^{13}C$ and proxy $\delta^{13}C$ data. The smallest error is found for an approximate doubling in the global mean efficiency of the biological pump $\overline{BP_{eff}}$ (from 38 % in the PI ocean to ~75 % in the LGM). Such a change minimizes the simulated global mean absolute error for $\delta^{13}C$ from 0.67 ‰ (for the originally simulated 33 % $\overline{BP_{eff}}$ of the LGM) to 0.26 ‰ - only distinguishable by 0.07 ‰ from the $\delta^{13}C$ data uncertainty. It additionally improves the agreement with both qualitative and quantitative O_2 reconstructions. Much of the remaining model-proxy $\delta^{13}C$ data mismatch is due to a too weak vertical chemocline in glacial simulations. Therefore, scaling of the biological pump efficiency does not fully explain the glacial ocean proxy data using the modelled circulation field thought to most closely represent the glacial state. We see different explanations of the bias that could strengthen the glacial chemocline, such as the further aging (by isolation and stratification) of interior waters through improved simulation of deep-water formation, which would increase the regenerated signature of the interior LGM ocean. Especially Southern Source Waters would have a large potential (due to their large volume contribution) to increase global interior radiocarbon ages and regenerated signatures of the interior ocean.

The estimated $\overline{BP_{eff}}$ increase to 75 % corresponds to an increase in oceanic DIC (ΔDIC) of ~1850 Gt C. This lies in the range of estimates as derived by the Bern3D Earth System Model of Intermediate Complexity constrained by single proxy targets (pCO$_2$^{atm}, δ^{13}C^{atm}, marine δ^{13}C of DIC, or deep equatorial Pacific CO$_3$$^{2-}$). If all four targets are used as constraints, the range of ΔDIC estimates based on the Bern3D model is higher than 1850 Gt C (see Fig. S3 and SM3). In order to disentangle and understand the processes contributing to ΔDIC, especially the large contribution from sedimentation-weathering imbalances, further work seems necessary.

The general agreement between our model results and proxy data for ocean circulation (within the uncertainty of reconstructions), after adjustments to the sea surface salinity field, demonstrates an advantage of our forced ocean model setup, and its flexibility, over fully coupled Earth System Models in exploring different circulation and biological pump scenarios for explaining glacial CO_2 changes. We conclude that a large PI-to-LGM increase in the efficiency of the biological pump (from 38 to ~75 %) as well as a reorganization of ocean circulation/stratification are essential for simulating an LGM ocean in optimal agreement with proxy data. Based on this, we expect that only fully coupled models that contain the processes and/or components that realistically change these aspects will be able to simulate an LGM ocean in satisfactory agreement with proxy data.

Data availability. The model output data for the PI and LGM simulations is available at the NIRD Research Data Archive (*AT PUBLICATION; DOI).*

Author contributions. ALM, JS and CH conceptualized the study and developed the methodology in cooperation with IB and contribution from AJT. ALM did the formal analysis of the data and wrote the original draft for which she visualized the results. ALM, JS, CH, AJT and UN investigated the results. All authors contributed to the review

and editing of the original draft. JS and ALM curated the data, contributed to the software and validated the results. CH and JS supervised the project, and provided the resources and funding acquisition needed for this work.

Competing interests. The authors declare that they have no conflict of interest.

Disclaimer. This article reflects only the authors' view – the funding agencies as well as their executive agencies are not responsible for any use that may be made of the information that the article contains.

Acknowledgments. This is a contribution to the Bjerknes Centre for Climate Research (Bergen, Norway). Storage and computing resources were provided by UNINETT Sigma2 - the National Infrastructure for High Performance Computing and Data Storage in Norway (project numbers nn/ns2980k and nn/ns2345k). AM is grateful for PhD funding through the Faculty for Mathematics and Natural Sciences of the University of Bergen (UoB) as well as support by the Meltzer fund of UoB and Erasmus Mundus to stay at ETH Zürich for part of this work. JS acknowledges funding through the Research Council of Norway (project INES 270061). The NorESM components were upgraded with support from project EVA (Earth system modelling of climate Variations in the Anthropocene, grant no. 229771, Research Council of Norway) and, CRESCENDO (Coordinated Research in Earth Systems and Climate: Experiments, kNowledge, Dissemination and Outreach; Horizon 2020 European Union's Framework Programme for Research and Innovation, grant no. 641816, European Commission). AJT acknowledges support from the Swiss National Science Foundation (# 200020_172476) and the Oeschger Centre for Climate Change Research.

References

Adkins J. F.: The role of deep ocean circulation in setting glacial climates, Paleoceanography, 28, 539-561, 10.1002/palo.20046, 2013.

Assmann, K. M., Bentsen, M., Segschneider, J., and Heinze, C.: An isopycnic ocean carbon cycle model, Geosci. Model Dev., 3, 143-167, 10.5194/gmd-3-143-2010, 2010.

EPICA Project Members: Eight glacial cycles from an Antarctic ice core, Nature, 429, 623-628, 10.1038/nature02599, 2004.

Bentsen, M., Bethke, I., Debernard, J. B., Iversen, T., Kirkevåg, A., Seland, Ø., Drange, H., Roelandt, C., Seierstad, I. A., Hoose, C., and Kristjánsson, J. E.: The Norwegian Earth System Model, NorESM1-M – Part 1: Description and basic evaluation of the physical climate, Geosci. Model Dev., 6, 687-720, 10.5194/gmd-6-687-2013, 2013.

Bereiter, B., Shackleton, S., Baggenstos, D., Kawamura, K., and Severinghaus, J.: Mean global ocean temperatures during the last glacial transition, Nature, 553, 39, 10.1038/nature25152, 2018.

Bopp, L., Resplandy, L., Untersee, A., Le Mezo, P., and Kageyama, M.: Ocean (de)oxygenation from the Last Glacial Maximum to the twenty-first century: insights from Earth System models, Philos Trans A Math Phys Eng Sci, 375, 20160323, 10.1098/rsta.2016.0323, 2017.

Bouttes, N., Paillard, D., Roche, D. M., Brovkin, V., and Bopp, L.: Last Glacial Maximum CO2 and δ^{13}C successfully reconciled, Geophysical Research Letters, 38, 10.1029/2010GL044499, 2011.

Braconnot, P., Harrison, S., Kageyama, M., Bartlein, P., Masson-Delmotte, V., Abe-Ouchi, A., Otto-Bliesner, B., and Zhao, Y.: Evaluation of climate models using palaeoclimatic data, Nature Climate Change, 2, 417-424, 10.1038/nclimate1456, 2012.

Broecker, W. S.: "NO", a conservative water-mass tracer, Earth and Planetary Science Letters, 23, 100-107, 10.1016/0012-821X(74)90036-3, 1974.

Broecker, W. S.: Glacial to interglacial changes in ocean chemistry, Progress in Oceanography, 11, 151-197, 10.1016/0079-6611(82)90007-6, 1982.

Broecker, W. S., and McGee, D.: The ^{13}C record for atmospheric CO_2: What is it trying to tell us?, Earth and Planetary Science Letters, 368, 175-182, 10.1016/j.epsl.2013.02.029, 2013.

5   Broecker, W. S., and Peng, T.-H.: Carbon Cycle: 1985 Glacial to Interglacial Changes in the Operation of the Global Carbon Cycle, Radiocarbon, 28, 309-327, 10.1017/S0033822200007414, 1986.

Buchanan, P. J., Matear, R. J., Lenton, A., Phipps, S. J., Chase, Z., and Etheridge, D. M.: The simulated climate of the Last Glacial Maximum and insights into the global marine carbon cycle, Climate of the Past, 12, 2271-2295, 10.5194/cp-12-2271-2016, 2016.

10   Burckel, P., Waelbroeck, C., Luo, Y., Roche, D. M., Pichat, S., Jaccard, S. L., Gherardi, J.-M., Govin, A., Lippold, J., and Thil, F.: The Atlantic Meridional Overturning Circulation during the last glacial. In: Supplement to: Burckel, P et al. (2016): Changes in the geometry and strength of the Atlantic meridional overturning circulation during the last glacial (20-50 ka). Climate of the Past, 12(11), 2061-2075, 10.5194/cp-12-2061-2016, PANGAEA, 2016.

15   Böhm, E., Lippold, J., Gutjahr, M., Frank, M., Blaser, P., Antz, B., Fohlmeister, J., Frank, N., Andersen, M. B., and Deininger, M.: Strong and deep Atlantic meridional overturning circulation during the last glacial cycle, Nature, 517, 73, 10.1038/nature14059, 2014.

Chowdhury, P., and Behera, M. R.: Evaluation of CMIP5 and CORDEX derived wave climate in Indian Ocean, Climate Dynamics, 52, 4463-4482, 10.1007/s00382-018-4391-0, 2019.

20   Costa, K. M., McManus, J. F., Anderson, R. F., Ren, H., Sigman, D. M., Winckler, G., Fleisher, M. Q., Marcantonio, F., and Ravelo, A. C.: No iron fertilization in the equatorial Pacific Ocean during the last ice age, Nature, 529, 519-522, 10.1038/nature16453, 2016.

Craig, H.: Isotopic standards for carbon and oxygen and correction factors for mass-spectrometric analysis of carbon dioxide, Geochimica et Cosmochimica Acta, 12, 133-149, 10.1016/0016-7037(57)90024-8, 1957.

25   Danabasoglu, G., Yeager, S. G., Bailey, D., Behrens, E., Bentsen, M., Bi, D., Biastoch, A., Böning, C., Bozec, A., Canuto, V. M., Cassou, C., Chassignet, E., Coward, A. C., Danilov, S., Diansky, N., Drange, H., Farneti, R., Fernandez, E., Fogli, P. G., Forget, G., Fujii, Y., Griffies, S. M., Gusev, A., Heimbach, P., Howard, A., Jung, T., Kelley, M., Large, W. G., Leboissetier, A., Lu, J., Madec, G., Marsland, S. J., Masina, S., Navarra, A., George Nurser, A. J., Pirani, A., y Mélia, D. S., Samuels, B. L., Scheinert, M., Sidorenko, D., Treguier, A.-M., Tsujino,

30   H., Uotila, P., Valcke, S., Voldoire, A., and Wang, Q.: North Atlantic simulations in Coordinated Ocean-ice Reference Experiments phase II (CORE-II). Part I: Mean states, Ocean Modelling, 73, 76-107, 10.1016/j.ocemod.2013.10.005, 2014.

De Boyer Montégut, C., Madec, G., Fischer, A. S., Lazar, A., and Iudicone, D.: Mixed layer depth over the global ocean: An examination of profile data and a profile-based climatology, Journal of Geophysical Research: Oceans,

35   109, 10.1029/2004JC002378, 2004.

DeVries, T., Primeau, F., and Deutsch, C.: The sequestration efficiency of the biological pump, Geophysical Research Letters, 39, L13601, 10.1029/2012GL051963, 2012.

Donohue, K. A., Tracey, K. L., Watts, D. R., Chidichimo, M. P., and Chereskin, T. K.: Mean Antarctic Circumpolar Current transport measured in Drake Passage, Geophysical Research Letters, 43, 11,760-711,767,

40   10.1002/2016GL070319, 2016.

Duplessy, J. C., Shackleton, N. J., Fairbanks, R. G., Labeyrie, L., Oppo, D., and Kallel, N.: Deepwater source variations during the last climatic cycle and their impact on the global deepwater circulation, Paleoceanography, 3, 343-360, 10.1029/PA003i003p00343, 1988.

Eide, M., Olsen, A., Ninnemann, U. S., and Johannessen, T.: A global ocean climatology of preindustrial and modern ocean $\delta^{13}C$, Global Biogeochemical Cycles, 31, 515-534, 10.1002/2016GB005473, 2017.

Ferrari, R., Jansen, M. F., Adkins, J. F., Burke, A., Stewart, A. L., and Thompson, A. F.: Antarctic sea ice control on ocean circulation in present and glacial climates, Proceedings of the National Academy of Sciences, 111, 8753, 10.1073/pnas.1323922111, 2014.

Filippelli, G. M., Latimer, J. C., Murray, R. W., and Flores, J.-A.: Productivity records from the Southern Ocean and the equatorial Pacific Ocean: Testing the glacial Shelf-Nutrient Hypothesis, Deep Sea Research Part II: Topical Studies in Oceanography, 54, 2443-2452, 10.1016/j.dsr2.2007.07.021, 2007.

Freeman, E., Skinner, L. C., Waelbroeck, C., and Hodell, D.: Radiocarbon evidence for enhanced respired carbon storage in the Atlantic at the Last Glacial Maximum, Nature Communications, 7, 11998, 10.1038/ncomms11998, 2016.

Ganopolski, A., and Brovkin, V.: Simulation of climate, ice sheets and CO_2 evolution during the last four glacial cycles with an Earth system model of intermediate complexity, Climate of the Past, 13, 1695-1716, 10.5194/cp-13-1695-2017, 2017.

Gebbie, G., and Huybers, P.: The Mean Age of Ocean Waters Inferred from Radiocarbon Observations: Sensitivity to Surface Sources and Accounting for Mixing Histories, Journal of Physical Oceanography, 42, 291-305, 10.1175/jpo-d-11-043.1, 2012.

Gebbie, G.: How much did Glacial North Atlantic Water shoal?, Paleoceanography, 29, 190-209, 10.1002/2013PA002557, 2014.

Gebbie, G., Peterson, C. D., Lisiecki, L. E., and Spero, H. J.: Global-mean marine $\delta^{13}C$ and its uncertainty in a glacial state estimate, Quaternary Science Reviews, 125, 144-159, 10.1016/j.quascirev.2015.08.010, 2015.

Gersonde, R., Crosta, X., Abelmann, A., and Armand, L.: Sea-surface temperature and sea ice distribution of the Southern Ocean at the EPILOG Last Glacial Maximum—a circum-Antarctic view based on siliceous microfossil records, Quaternary Science Reviews, 24, 869-896, 10.1016/j.quascirev.2004.07.015, 2005.

Gottschalk, J., Skinner, L. C., Lippold, J., Vogel, H., Frank, N., Jaccard, S. L., and Waelbroeck, C.: Biological and physical controls in the Southern Ocean on past millennial-scale atmospheric CO_2 changes, Nature Communications, 7, 11539, 10.1038/ncomms11539, 2016a.

Gottschalk, J., Vázquez Riveiros, N., Waelbroeck, C., Skinner, L. C., Michel, E., Duplessy, J.-C., Hodell, D. A., and Mackensen, A.: Stable oxygen and carbon isotopes of C. wuellerstorfi, C. kullenbergi and Uvigerina spp. from MD07-3076Q (sub-Antarctic Atlantic) over the last 22 kyrs. In: In supplement to: Gottschalk, J et al. (2016): Carbon isotope offsets between benthic foraminifer species of the genus Cibicides (Cibicidoides) in the glacial sub-Antarctic Atlantic. Paleoceanography, 31(12), 1583-1602, 10.1002/2016PA003029, PANGAEA, 2016b.

Gottschalk, J., Vázquez Riveiros, N., Waelbroeck, C., Skinner, L. C., Michel, E., Duplessy, J.-C., Hodell, D. A., and Mackensen, A.: Stable oxygen and carbon isotopes of C. wuellerstorfi, C. kullenbergi and Uvigerina spp. from TN057-6GC (sub-Antarctic Atlantic) over the last 29 kyrs. In: In supplement to: Gottschalk, J et al. (2016): Carbon isotope offsets between benthic foraminifer species of the genus Cibicides (Cibicidoides) in the glacial sub-Antarctic Atlantic. Paleoceanography, 31(12), 1583-1602, 10.1002/2016PA003029, PANGAEA, 2016c.

Gruber, N., Keeling, C. D., Bacastow, R. B., Guenther, P. R., Lueker, T. J., Wahlen, M., Meijer, H. A. J., Mook, W. G., and Stocker, T. F.: Spatiotemporal patterns of carbon-13 in the global surface oceans and the oceanic suess effect, Global Biogeochemical Cycles, 13, 307-335, 10.1029/1999GB900019, 1999.

Guo, C., Bentsen, M., Bethke, I., Ilicak, M., Tjiputra, J., Toniazzo, T., Schwinger, J., and Otterå, O. H.: Description and evaluation of NorESM1-F: a fast version of the Norwegian Earth System Model (NorESM), Geoscientific Model Development, 12, 343-362, 10.5194/gmd-12-343-2019, 2019.

Heinze, C., Maier-Reimer, E., and Winn, K.: Glacial pCO_2 Reduction by the World Ocean: Experiments With the Hamburg Carbon Cycle Model, Paleoceanography, 6, 395-430, 10.1029/91PA00489, 1991.

Heinze, C., and Hasselmann, K.: Inverse Multiparameter Modeling of Paleoclimate Carbon Cycle Indices, Quaternary Research, 40, 281-296, 10.1006/qres.1993.1082, 1993.

Heinze, C., Hoogakker, B. A. A., and Winguth, A.: Ocean carbon cycling during the past 130 000 years – a pilot study on inverse palaeoclimate record modelling, Climate of the Past, 12, 1949-1978, 10.5194/cp-12-1949-2016, 2016.

Ho, S., and Laepple, T.: Glacial cooling as inferred from marine temperature proxies TEXH86 and UK′37, Earth and Planetary Science Letters, 409, 15-22, 10.1016/j.epsl.2014.10.033, 2015.

Hodell, D. A., and Channell, J. E. T.: Stable isotope ratios of Cibicidoides wuellerstorfi from IODP Site 303-U1304. In: In supplement to: Hodell, DA; Channell, JET (2016): Mode transitions in Northern Hemisphere glaciation: co-evolution of millennial and orbital variability in Quaternary climate. Climate of the Past, 12(9), 1805-1828, 10.5194/cp-12-1805-2016, PANGAEA, 2016.

Howe, J. N. W., and Piotrowski, A. M.: (Table S2) Stable carbon and oxygen isotopic composition of benthic foraminifera of ODP Site 154-929. In: In supplement to: Howe, JNW; Piotrowski, AM: Atlantic deep water provenance decoupled from atmospheric CO_2 concentration during the lukewarm interglacials. Nature Communications, 10.1038/s41467-017-01939-w, PANGAEA, 2017.

Ito, T., Follows, M. J., and Boyle, E. A.: Is AOU a good measure of respiration in the oceans?, Geophysical Research Letters, 31, 10.1029/2004GL020900, 2004.

Ito, T., and Follows, M. J.: Preformed phosphate, soft tissue pump and atmospheric CO_2, Journal of Marine Research, 63, 813-839, 10.1357/0022240054663231, 2005.

Jaccard, S. L., Galbraith, E. D., Sigman, D. M., Haug, G. H., Francois, R., Pedersen, T. F., Dulski, P., and Thierstein, H. R.: Subarctic Pacific evidence for a glacial deepening of the oceanic respired carbon pool, Earth and Planetary Science Letters, 277, 156-16510.1016/j.epsl.2008.10.017, 2009.

Jaccard, S. L., and Galbraith, E. D.: Large climate-driven changes of oceanic oxygen concentrations during the last deglaciation, Nature Geoscience, 5, 151, 10.1038/ngeo1352, 2011.

Jansen, M. F.: Glacial ocean circulation and stratification explained by reduced atmospheric temperature, Proceedings of the National Academy of Sciences, 114, 45-50, 10.1073/pnas.1610438113, 2017.

Jeltsch-Thömmes, A., Battaglia, G., Cartapanis, O., Jaccard, S. L., and Joos, F.: Low terrestrial carbon storage at the Last Glacial Maximum: constraints from multi-proxy data, Climate of the Past, 15, 849-879, 10.5194/cp-15-849-2019, 2019.

Kageyama, M., Albani, S., Braconnot, P., Harrison, S. P., Hopcroft, P. O., Ivanovic, R. F., Lambert, F., Marti, O., Peltier, W. R., Peterschmitt, J. Y., Roche, D. M., Tarasov, L., Zhang, X., Brady, E. C., Haywood, A. M., LeGrande, A. N., Lunt, D. J., Mahowald, N. M., Mikolajewicz, U., Nisancioglu, K. H., Otto-Bliesner, B. L., Renssen, H.,

Tomas, R. A., Zhang, Q., Abe-Ouchi, A., Bartlein, P. J., Cao, J., Li, Q., Lohmann, G., Ohgaito, R., Shi, X., Volodin, E., Yoshida, K., Zhang, X., and Zheng, W.: The PMIP4 contribution to CMIP6 – Part 4: Scientific objectives and experimental design of the PMIP4-CMIP6 Last Glacial Maximum experiments and PMIP4 sensitivity experiments, Geoscientific Model Development, 10, 4035-4055, 10.5194/gmd-10-4035-2017, 2017.

5 Khatiwala, S., Schmittner, A., and Muglia, J.: Air-sea disequilibrium enhances ocean carbon storage during glacial periods, Science Advances, 5, eaaw4981, 10.1126/sciadv.aaw4981, 2019.

Key, R. M., Kozyr, A., Sabine, C. L., Lee, K., Wanninkhof, R., Bullister, J. L., Feely, R. A., Millero, F. J., Mordy, C., and Peng, T. H.: A global ocean carbon climatology: Results from Global Data Analysis Project (GLODAP), Global Biogeochemical Cycles, 18, GB4031, 10.1029/2004GB002247, 2004.

10 Kohfeld, K. E., Quéré, C. L., Harrison, S. P., and Anderson, R. F.: Role of Marine Biology in Glacial-Interglacial CO_2 Cycles, Science, 308, 74-78, 10.1126/science.1105375, 2005.

Kurahashi-Nakamura, T., Paul, A., and Losch, M.: Dynamical reconstruction of the global ocean state during the Last Glacial Maximum, Paleoceanography, 32, 326-350, 10.1002/2016PA003001, 2017.

Lamy, F., Arz, H. W., Kilian, R., Lange, C. B., Lembke-Jene, L., Wengler, M., Kaiser, J., Baeza-Urrea, O., Hall, 15 I. R., Harada, N., and Tiedemann, R.: Glacial reduction and millennial-scale variations in Drake Passage throughflow, Proceedings of the National Academy of Sciences, 112, 13496, 10.1073/pnas.1509203112, 2015.

Laws, E. A., Bidigare, R., R., and Popp, B. N.: Effects of growth rate and CO_2 concentration on carbon isotopic fractionation by the marine diatom Phaeodactylum tricornutum, Limnology and Oceanography, 42, 1552-1560, 10.4319/lo.1997.42.7.1552, 1997.

20 Lynch-Stieglitz, J., Stocker, T. F., Broecker, W. S., and Fairbanks, R. G.: The influence of air-sea exchange on the isotopic composition of oceanic carbon: Observations and modeling, Global Biogeochemical Cycles, 9, 653-665, 10.1029/95GB02574, 1995.

Lynch-Stieglitz, J., Adkins, J. F., Curry, W. B., Dokken, T., Hall, I. R., Herguera, J. C., Hirschi, J. J. M., Ivanova, E. V., Kissel, C., Marchal, O., Marchitto, T. M., McCave, I. N., McManus, J. F., Mulitza, S., Ninnemann, U., 25 Peeters, F., Yu, E.-F., and Zahn, R.: Atlantic Meridional Overturning Circulation During the Last Glacial Maximum, Science, 316, 66, 10.1126/science.1137127, 2007.

Lynch-Stieglitz, J., Ito, T., and Michel, E.: Antarctic density stratification and the strength of the circumpolar current during the Last Glacial Maximum, Paleoceanography, 31, 539-552, 10.1002/2015PA002915, 2016.

Mahowald, N. M., Muhs, D. R., Levis, S., Rasch, P. J., Yoshioka, M., Zender, C. S., and Luo, C.: Change in 30 atmospheric mineral aerosols in response to climate: Last glacial period, preindustrial, modern, and doubled carbon dioxide climates, Journal of Geophysical Research: Atmospheres, 111, 10.1029/2005JD006653, 2006.

Maier-Reimer, E.: Geochemical cycles in an ocean general circulation model. Preindustrial tracer distributions, Global Biogeochemical Cycles, 7, 645-677, 10.1029/93GB01355, 1993.

Maier-Reimer, E., Kriest, I., Segschneider, J., and Wetzel, P.: The Hamburg Oceanic Carbon Cycle Circulation 35 model HAMOCC5.1 – Technical Description Release 1.1, Max Planck Institute for Meteorology, Hamburg, Germany, 2005.

Marchitto, T. M., and Broecker, W. S.: Deep water mass geometry in the glacial Atlantic Ocean: A review of constraints from the paleonutrient proxy Cd/Ca, Geochemistry, Geophysics, Geosystems, 7, 10.1029/2006GC001323, 2006.

MARGO Project Members: Constraints on the magnitude and patterns of ocean cooling at the Last Glacial Maximum, Nature Geoscience, 2, 127, 10.1038/ngeo411, 2009.

Marzocchi, A., and Jansen, M. F.: Connecting Antarctic sea ice to deep-ocean circulation in modern and glacial climate simulations, Geophysical Research Letters, 44, 6286-6295, 10.1002/2017GL073936, 2017.

5   Mazaud, A., Michel, E., Dewilde, F., and Turon, J. L.: Variations of the Antarctic Circumpolar Current intensity during the past 500 ka, Geochemistry, Geophysics, Geosystems, 11, 10.1029/2010GC003033, 2010.

McCarthy, G. D., Smeed, D. A., Johns, W. E., Frajka-Williams, E., Moat, B. I., Rayner, D., Baringer, M. O., Meinen, C. S., Collins, J., and Bryden, H. L.: Measuring the Atlantic Meridional Overturning Circulation at 26°N, Progress in Oceanography, 130, 91-111, 10.1016/j.pocean.2014.10.006, 2015.

10   McCave, I. N., Crowhurst, S. J., Kuhn, G., Hillenbrand, C. D., and Meredith, M. P.: Minimal change in Antarctic Circumpolar Current flow speed between the last glacial and Holocene, Nature Geoscience, 7, 113, 10.1038/ngeo2037, 2013.

McManus, J. F., Francois, R., Gherardi, J. M., Keigwin, L. D., and Brown-Leger, S.: Collapse and rapid resumption of Atlantic meridional circulation linked to deglacial climate changes, Nature, 428, 834-837, 10.1038/nature02494, 15   2004.

Menviel, L., Yu, J., Joos, F., Mouchet, A., Meissner, K. J., and England, M. H.: Poorly ventilated deep ocean at the Last Glacial Maximum inferred from carbon isotopes: A data-model comparison study, Paleoceanography, 32, 2-17, 10.1002/2016pa003024, 2017.

Mitchell, D., AchutaRao, K., Allen, M., Bethke, I., Beyerle, U., Ciavarella, A., Forster, P. M., Fuglestvedt, J., 20   Gillett, N., Haustein, K., Ingram, W., Iversen, T., Kharin, V., Klingaman, N., Massey, N., Fischer, E., Schleussner, C. F., Scinocca, J., Seland, Ø., Shiogama, H., Shuckburgh, E., Sparrow, S., Stone, D., Uhe, P., Wallom, D., Wehner, M., and Zaaboul, R.: Half a degree additional warming, prognosis and projected impacts (HAPPI): background and experimental design, Geosci. Model Dev., 10, 571-583, 10.5194/gmd-10-571-2017, 2017.

Molina-Kescher, M., Frank, M., Tapia, R., Ronge, T. A., Nürnberg, D., and Tiedemann, R.: Radiogenic 25   neodymium, strontium and lead isotopes of authigenic and detrital sedimentary phases and stable oxygen and carbon isotopes of benthic foraminifera from gravity cores SO213-59-2 and SO213-60-1 (central South Pacific). In: Supplement to: Molina-Kescher, M et al. (2016): Reduced admixture of North Atlantic Deep Water to the deep central South Pacific during the last two glacial periods. Paleoceanography, 10.1002/2015PA002863, PANGAEA, 2016.

30   Mook, W. G.: ^{13}C in atmospheric CO_2, Netherlands Journal of Sea Research, 20, 211-223, 10.1016/0077-7579(86)90043-8, 1986.

Morée, A. L., Schwinger, J., and Heinze, C.: Southern Ocean controls of the vertical marine δ^{13}C gradient – a modelling study, Biogeosciences, 15, 7205-7223, 10.5194/bg-15-7205-2018, 2018.

Morée, A. L., and Schwinger, J.: A Last Glacial Maximum forcing dataset for ocean modelling, Earth Syst. Sci. 35   Data Discuss., 2019, 1-14, 10.5194/essd-2019-79, 2019.

Moy, A. D., Palmer, M. R., Howard, W. R., Bijma, J., Cooper, M. J., Calvo, E., Pelejero, C., Gagan, M. K., and Chalk, T. B.: Varied contribution of the Southern Ocean to deglacial atmospheric CO_2 rise, Nature Geoscience, 10.1038/s41561-019-0473-9, 2019.

Muglia, J., and Schmittner, A.: Glacial Atlantic overturning increased by wind stress in climate models, 40   Geophysical Research Letters, 42, 9862-9868, 10.1002/2015gl064583, 2015.

Muglia, J., Skinner, L. C., and Schmittner, A.: Weak overturning circulation and high Southern Ocean nutrient utilization maximized glacial ocean carbon, Earth and Planetary Science Letters, 496, 47-56, 10.1016/j.epsl.2018.05.038, 2018.

5 Nadeau, L.-P., Ferrari, R., and Jansen, M. F.: Antarctic Sea Ice Control on the Depth of North Atlantic Deep Water, Journal of Climate, 32, 2537-2551, 10.1175/JCLI-D-18-0519.1, 2019.

Oka, A., Abe-Ouchi, A., Chikamoto, M. O., and Ide, T.: Mechanisms controlling export production at the LGM: Effects of changes in oceanic physical fields and atmospheric dust deposition, Global Biogeochemical Cycles, 25, 10.1029/2009GB003628, 2011.

Oliver, K. I. C., Hoogakker, B. A. A., Crowhurst, S., Henderson, G. M., Rickaby, R. E. M., Edwards, N. R., and 10 Elderfield, H.: A synthesis of marine sediment core δ^{13}C data over the last 150 000 years, Climate of the Past, 6, 645-673, 10.5194/cp-6-645-2010, 2010.

Oppo, D. W., Gebbie, G., Huang, K.-F., Curry, W. B., Marchitto, T. M., and Pietro, K. R.: Data Constraints on Glacial Atlantic Water Mass Geometry and Properties, Paleoceanography and Paleoclimatology, 33, 1013-1034, 10.1029/2018PA003408, 2018.

15 Peterson, C. D., Lisiecki, L. E., and Stern, J. V.: Deglacial whole-ocean δ^{13}C change estimated from 480 benthic foraminiferal records, Paleoceanography, 29, 549-563, 10.1002/2013PA002552, 2014.

Primeau, F. W., Holzer, M., and DeVries, T.: Southern Ocean nutrient trapping and the efficiency of the biological pump, Journal of Geophysical Research: Oceans, 118, 2547-2564, 10.1002/jgrc.20181, 2013.

Rahmstorf, S.: On the freshwater forcing and transport of the Atlantic thermohaline circulation, Climate Dynamics, 20 12, 799-811, 10.1007/s003820050144, 1996.

Roche, D. M., Crosta, X., and Renssen, H.: Evaluating Southern Ocean sea-ice for the Last Glacial Maximum and pre-industrial climates: PMIP-2 models and data evidence, Quaternary Science Reviews, 56, 99-106, 10.1016/j.quascirev.2012.09.020, 2012.

Sarmiento, J. L., Gruber, N., Brzezinski, M. A., and Dunne, J. P.: High-latitude controls of thermocline nutrients 25 and low latitude biological productivity, Nature, 427, 56-60, 10.1038/nature02127, 2004.

Sarmiento, J. L., and Gruber, N.: Ocean biogeochemical dynamics, Princeton University Press Princeton, 2006.

Schmitt, J., Schneider, R., Elsig, J., Leuenberger, D., Lourantou, A., Chappellaz, J., Köhler, P., Joos, F., Stocker, T. F., Leuenberger, M., and Fischer, H.: Carbon Isotope Constraints on the Deglacial CO_2 Rise from Ice Cores, Science, 336, 711-714, 10.1126/science.1217161, 2012.

30 Schmittner, A., Gruber, N., Mix, A. C., Key, R. M., Tagliabue, A., and Westberry, T. K.: Biology and air-sea gas exchange controls on the distribution of carbon isotope ratios (δ^{13}C) in the ocean, Biogeosciences, 10, 5793-5816, 10.5194/bg-10-5793-2013, 2013.

Schmittner, A., and Somes, C. J.: Complementary constraints from carbon (^{13}C) and nitrogen (^{15}N) isotopes on the glacial ocean's soft-tissue biological pump, Paleoceanography, 31, 669-693, 10.1002/2015PA002905, 2016.

35 Schwinger, J., Goris, N., Tjiputra, J. F., Kriest, I., Bentsen, M., Bethke, I., Ilicak, M., Assmann, K. M., and Heinze, C.: Evaluation of NorESM-OC (versions 1 and 1.2), the ocean carbon-cycle stand-alone configuration of the Norwegian Earth System Model (NorESM1), Geoscientific Model Development, 9, 2589-2622, 10.5194/gmd-9-2589-2016, 2016.

Sigman, D. M., and Boyle, E. A.: Glacial/interglacial variations in atmospheric carbon dioxide, Nature, 407, 859-40 869, 10.1038/35038000, 2000.

Sigman, D. M., Hain, M. P., and Haug, G. H.: The polar ocean and glacial cycles in atmospheric CO_2 concentration, Nature, 466, 47, 10.1038/nature09149, 2010.

Sikes, E. L., Elmore, A. C., Allen, K. A., Cook, M. S., and Guilderson, T. P.: Glacial water mass structure and rapid $\delta^{18}O$ and $\delta^{13}C$ changes during the last glacial termination in the Southwest Pacific, Earth and Planetary Science Letters, 456, 87-97, 10.1016/j.epsl.2016.09.043, 2016.

Skinner, L. C., Primeau, F., Freeman, E., de la Fuente, M., Goodwin, P. A., Gottschalk, J., Huang, E., McCave, I. N., Noble, T. L., and Scrivner, A. E.: Radiocarbon constraints on the glacial ocean circulation and its impact on atmospheric CO_2, Nature Communications, 8, 16010, 10.1038/ncomms16010, 2017.

Spence, J. P., Eby, M., and Weaver, A. J.: The Sensitivity of the Atlantic Meridional Overturning Circulation to Freshwater Forcing at Eddy-Permitting Resolutions, Journal of Climate, 21, 2697-2710, 10.1175/2007JCLI2103.1, 2008.

Srokosz, M. A., and Bryden, H. L.: Observing the Atlantic Meridional Overturning Circulation yields a decade of inevitable surprises, Science, 348, 10.1126/science.1255575, 2015.

Stephens, B. B., and Keeling, R. F.: The influence of Antarctic sea ice on glacial–interglacial CO_2 variations, Nature, 404, 171-174, 10.1038/35004556, 2000.

Takahashi, T., Broecker, W. S., and Langer, S.: Redfield ratio based on chemical data from isopycnal surfaces, Journal of Geophysical Research: Oceans, 90, 6907-6924, 10.1029/JC090iC04p06907, 1985.

Tamburini, F., and Föllmi, K. B.: Phosphorus burial in the ocean over glacial-interglacial time scales, Biogeosciences, 6, 501-513, 10.5194/bg-6-501-2009, 2009.

Tjiputra, J. F., Roelandt, C., Bentsen, M., Lawrence, D. M., Lorentzen, T., Schwinger, J., Seland, Ø., and Heinze, C.: Evaluation of the carbon cycle components in the Norwegian Earth System Model (NorESM), Geoscientific Model Development 6, 301-325, 10.5194/gmd-6-301-2013, 2013.

Tjiputra, J. F., Schwinger, J., Bentsen, M., Morée, A. L., Gao, S., Bethke, I., Heinze, C., Goris, N., Gupta, A., He, Y., Olivié, D., Seland, Ø., and Schulz, M.: Ocean biogeochemistry in the Norwegian Earth System Model version 2 (NorESM2), Geosci. Model Dev. Discuss., 2020, 1-64, 10.5194/gmd-2019-347, 2020.

Umling, N. E., Thunell, R. C., and Bizimis, M.: Deepwater Expansion and Enhanced Remineralization in the Eastern Equatorial Pacific During the Last Glacial Maximum, Paleoceanography and Paleoclimatology, 33, 563-578, 10.1029/2017PA003221, 2018.

Volk, T., and Hoffert, M. I.: Ocean Carbon Pumps: Analysis of Relative Strengths and Efficiencies in Ocean-Driven Atmospheric CO_2 Changes, in: The Carbon Cycle and Atmospheric CO_2: Natural Variations Archean to Present, American Geophysical Union, 99-110, 1985.

Weber, S. L., Drijfhout, S. S., Abe-Ouchi, A., Crucifix, M., Eby, M., Ganopolski, A., Murakami, S., Otto-Bliesner, B., and Peltier, W. R.: The modern and glacial overturning circulation in the Atlantic ocean in PMIP coupled model simulations, Climate of the Past, 3, 51-64, 10.5194/cp-3-51-2007, 2007.

Winckler, G., Anderson, R. F., Jaccard, S. L., and Marcantonio, F.: Ocean dynamics, not dust, have controlled equatorial Pacific productivity over the past 500,000 years, Proceedings of the National Academy of Sciences, 113, 6119, 10.1073/pnas.1600616113, 2016.

Winguth, A. M. E., Archer, D., Duplessy, J. C., Maier-Reimer, E., and Mikolajewicz, U.: Sensitivity of paleonutrient tracer distributions and deep-sea circulation to glacial boundary conditions, Paleoceanography, 14, 304-323, 10.1029/1999PA900002, 1999.

Yu, J., Menviel, L., Jin, Z. D., Thornalley, D. J. R., Barker, S., Marino, G., Rohling, E. J., Cai, Y., Zhang, F., Wang, X., Dai, Y., Chen, P., and Broecker, W. S.: Sequestration of carbon in the deep Atlantic during the last glaciation, Nature Geoscience, 9, 319-324, 10.1038/ngeo2657, 2016.

Yu, J., Menviel, L., Jin, Z. D., Thornalley, D. J. R., Foster, G. L., Rohling, E. J., McCave, I. N., McManus, J. F.,
5 Dai, Y., Ren, H., He, F., Zhang, F., Chen, P. J., and Roberts, A. P.: More efficient North Atlantic carbon pump during the Last Glacial Maximum, Nature Communications, 10, 2170, 10.1038/s41467-019-10028-z, 2019.

Zeebe, R., and Wolf-Gladrow, D.: CO_2 in Seawater: Equilibrium, Kinetics, Isotopes, Elsevier Oceanography Series, edited by: Halpern, D., Elsevier Science B.V., Amsterdam, The Netherlands, 346 pp., 2001.

Zhang, J., Quay, P. D., and Wilbur, D. O.: Carbon isotope fractionation during gas-water exchange and dissolution
10 of CO_2, Geochimica et Cosmochimica Acta, 59, 107-114, 10.1016/0016-7037(95)91550-D, 1995.

Ödalen, M., Nycander, J., Oliver, K. I. C., Brodeau, L., and Ridgwell, A.: The influence of the ocean circulation state on ocean carbon storage and CO_2 drawdown potential in an Earth system model, Biogeosciences, 15, 1367-1393, 10.5194/bg-15-1367-2018, 2018.
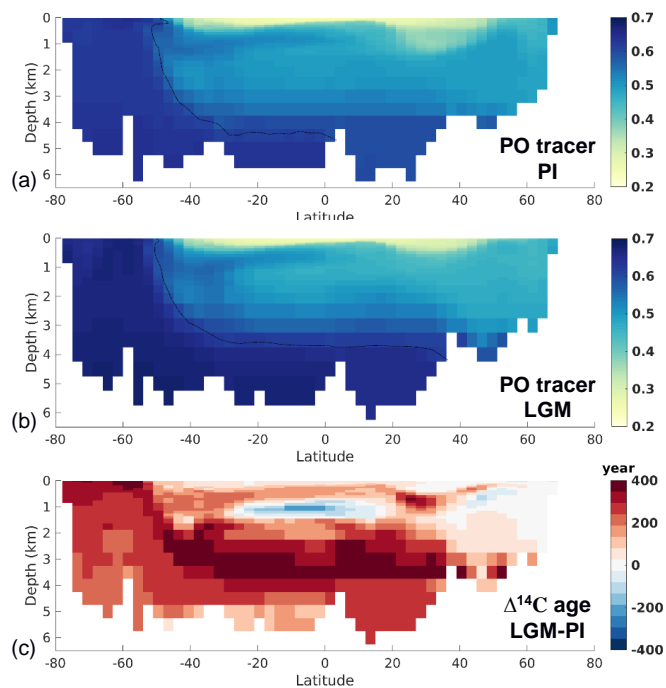
Figure 1 Atlantic zonal mean PO (25-35° W) for (a) the PI and (b) the LGM model states. PO = O$_2$ + 172 * PO$_4$ (Broecker, 1974). The line represents the respective end-member PO of the Southern source waters (mean Southern Ocean surface PO), and thus the extent of Southern source water. (c) The change in radiocarbon age between the LGM and PI. See Fig. S4 for the corresponding Pacific zonal mean transects.
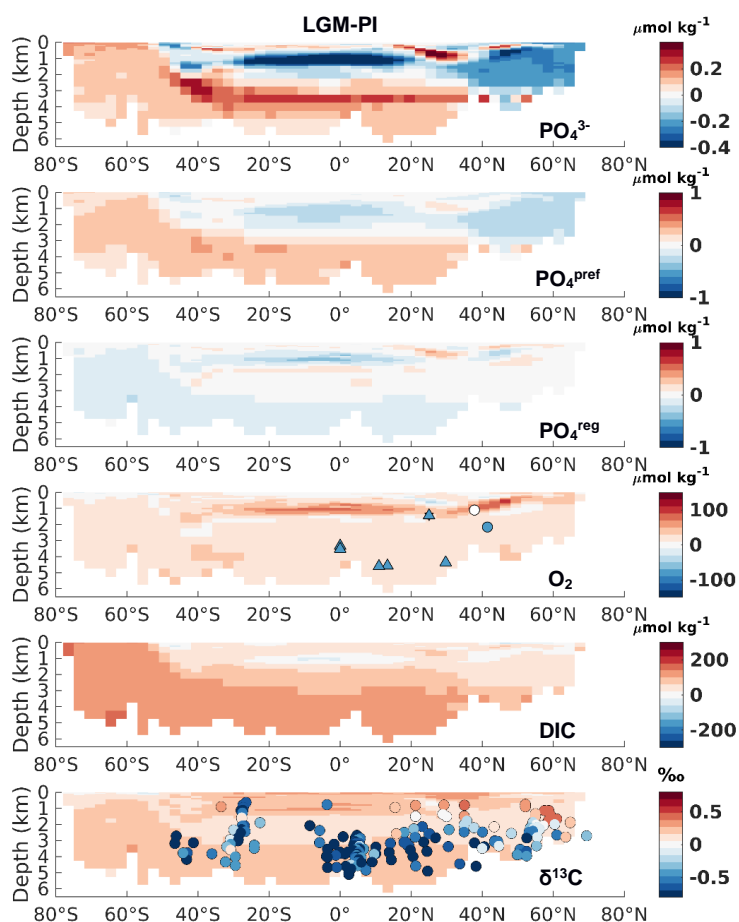
Figure 2 Atlantic zonal mean (25-35° W) of LGM-PI changes for the original model output. See Fig. S10 for the corresponding Pacific sections. Overlay on O₂ is qualitative estimates of LGM-PI changes in O₂ within 30° from 30° W, with blue being a decrease, white indicating unclear changes and red indicating an increase in O₂ (Jaccard and Galbraith, 2011). Simulated LGM-PI δ¹³C is compared to a compilation of LGM minus Late Holocene δ¹³C data within 30° from 30° W (Peterson et al., 2014; Muglia et al., 2018; Molina-Kescher et al., 2016; Sikes et al., 2016; Burckel et al., 2016; Gottschalk et al., 2016b-c; Hodell and Channell, 2016; Howe and Piotrowski, 2017).
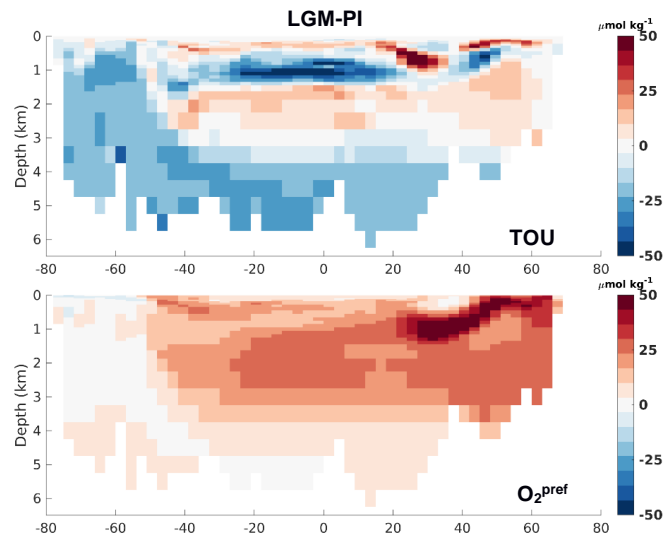
Figure 3 Atlantic zonal mean of simulated LGM-PI O$_2$ components True Oxygen Utilization (TOU= O$_2^{pref}$- O$_2$) (Ito et al., 2004) and preformed O$_2$ (O$_2^{pref}$), which is simulated as the O$_2$ concentration that leaves the surface ocean, and is thus different from saturated O$_2$ (Tjiputra et al., 2020).
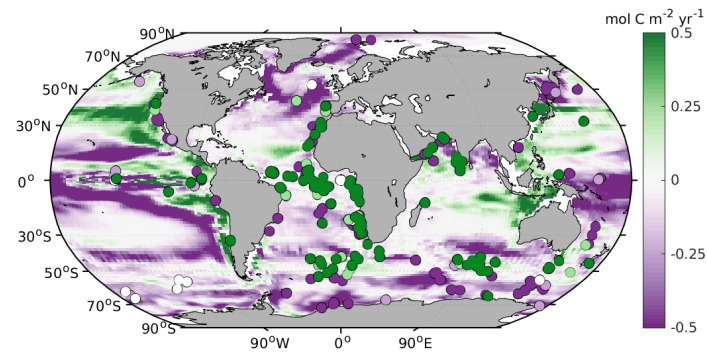
Figure 4 Comparison between the simulated LGM-PI change in export production at 100m depth and Kohfeld et al. (2005) qualitative data (dots: dark purple=decrease, light purple=small decrease, white=no change, light green=light increase, dark green=increase).
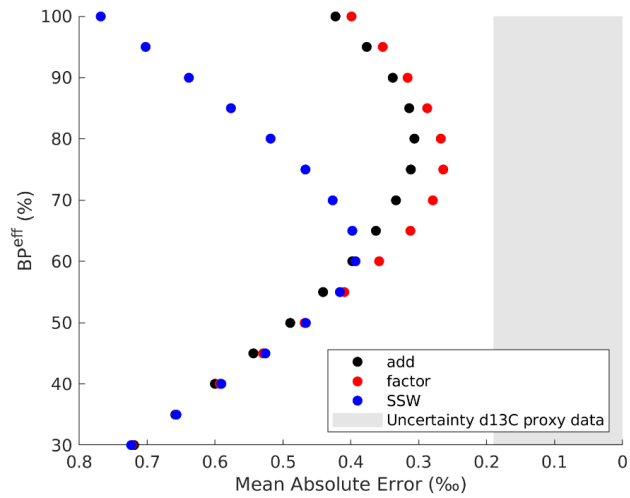
Figure 5 Efficiency of the biological pump ($\overline{BP_{eff}}$) versus the mean absolute error between all δ¹³C proxy data and the nearest model grid-cell δ¹³C, for different methods (Sect. 2.4). Note that the original LGM $\overline{BP_{eff}}$ is 33 %. The δ¹³C sediment core data have an uncertainty of ~0.19‰, shaded in grey (Peterson et al., 2014).
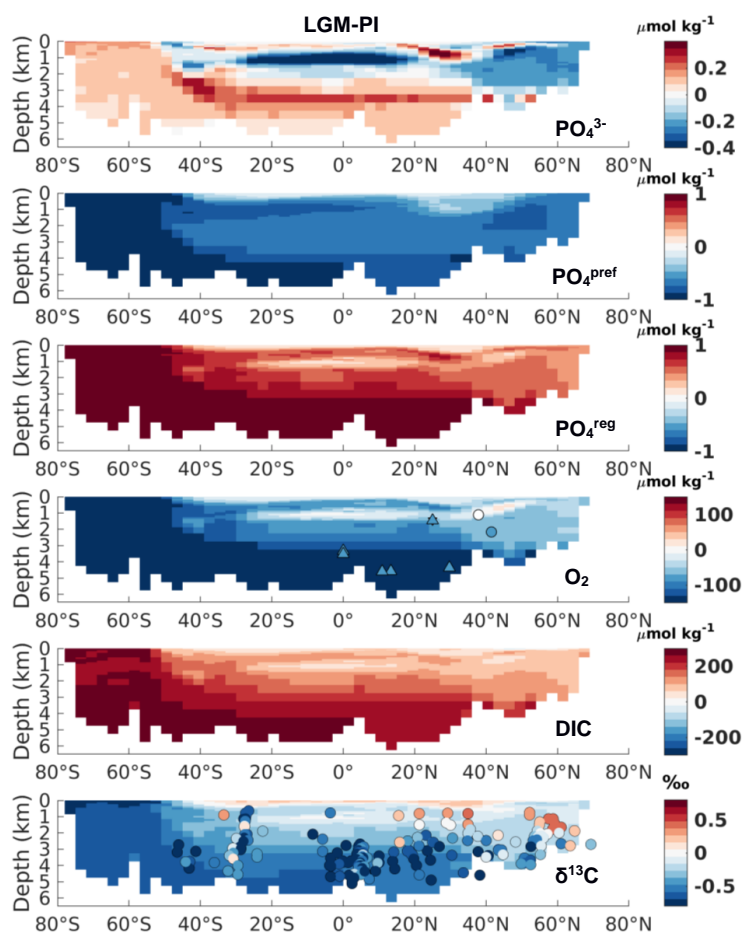
Figure 6 As Figure 2, but for an adjusted $\overline{BP_{eff}}$ of 75 %.